International Journal of Applied Mechanics
Vol. 14, No. 1 (2022) 2150124 (24 pages)

DOI: 10.1142/S1758825121501246

Nonlinear Mechanics of a Smart Biotensegrity Human Foot Prosthesis

Alex Brandão* and Marcelo A. Savi†

Universidade Federal do Rio de Janeiro
COPPE – Department of Mechanical Engineering
Center for Nonlinear Mechanics – MECANON
P. O. Box – 68.503, 21.941.972
Rio de Janeiro, RJ, Brazil
**alexbrandao@mecanica.coppe.ufrj.br*
†*savi@mecanica.coppe.ufrj.br*

Received 24 September 2021
Accepted 13 December 2021
Published 7 February 2022

This work deals with the nonlinear mechanics of smart bioinspired tensegrity structures. A minimal regular tensegrity prism actuated by shape memory alloy (SMA) elements is investigated to represent a human foot. A formulation considering the force density matrix approach is used to model the equilibrium equations of the tensegrity structure based on node mapping. Lagrange multipliers are employed to represent constraints. The SMA thermomechanical behavior is described by considering a modified polynomial constitutive model. Numerical simulations are developed from an optimization procedure employing the Levenberg–Marquardt method. An investigation of the tensegrity capability to model a human foot is carried out analyzing either mechanical or physiological aspects of the tensegrity prosthesis. The mechanical performance is compared with high performance prostheses available on the market, showing that it is an interesting alternative with respect to mechanical resistance. Regarding physiology, foot movements are properly mimicked from SMA actuation.

Keywords: Biotensegrity; prismatic simplex tensegrity; bioinspiration; prosthesis; foot; shape memory alloys.

1. Introduction

Tensegrity structures have a growing interest due to their mechanical and bioinspired characteristics. In brief, tensegrity structures are composed by bars (struts) and cables (strings) that are, respectively, subjected to compression and tension. After more than fifty years since the first tensegrity has appeared, there is still not a cabal definition of it, but it is usually defined as "islands of compression in an ocean of tension" [Buckminster Fuller, 1962]. Bioinspired systems are treated by different approaches [Benyus, 1997; Passino, 2006] and the use of tensegrity structures to

†Corresponding author.

represent biological systems is often called biotensegrity [Motro, 2003; Skelton and Oliveira, 2009; Zhang and Ohsaki, 2015; Hutson and Ward, 2016].

Skelton and Oliveira [2009] stated that the goal of the tensegrity structure design, although not mandatory, is to assure that the members are unidirectionally loaded, in such a way that members do not serve both compressive and tensile functions. Deepak Bansod *et al.* [2014] presented an overview of tensegrity structures highlighting their main features as being self-standing modulated structures with a higher load-bearing capacity with similar weight or as being lightweight with similar resistance if compared to conventional structures.

Tensegrity structure applications have been increasing in a large variety of fields. Termonia [1994] and Simmons *et al.* [1996] analyzed the spider silk respectively using magnetic resonance and X-Ray data. Vera *et al.* [2005] developed a mesoscale tensegrity structure to model one cell of 33 thousand cells to study the erythrocyte (red blood cell). Cañadas *et al.* [2002] and Sultan *et al.* [2004] employed tensegrity to model living cells. Ekeberg and Pearson [2005] performed computer simulations to study the physiology of cat's hind legs. A tensegrity-like 3D structure was employed with controllers to actuate two different signals: one force related to the ankle extensors; and another related to the angle at the hip joint. Scarr [2011] experimentally examined an elbow from a tensegrity perspective, where it is considered a uniaxial hinge rotation with pivot of proximal forearm rotation. The motions of the elbow are guided by the joint surfaces, while the ligaments serve the purpose of maintain structural integrity and the muscles drive the motion. Sun *et al.* [2019] employed the tensegrity concept to model a robotic foot for the purpose of adaptive locomotion on complex terrain, without control, with improved deformability, impact resistance and adaptability to environmental solicitations.

Smart materials present remarkable properties defined by the coupling of different physical fields, which allows the control through external stimuli, such as stress, temperature, magnetic field, electric current and others. Adaptive behavior makes these materials interesting candidates for bioinspired applications, being of special interest to work in consonance with tensegrities in order to mimic natural systems. In this regard, shape memory alloys (SMAs) present a thermomechanical coupling associated with solid-phase transformations, which allows the recovery of original shapes after large deformations, within the order of 10%. Savi *et al.* [2016] presented a general overview of shape memory alloys, showing theoretical background, main applications, and constitutive modeling.

SMA bioinspired applications have been increasing in a variety of fields and the literature has several examples that show the trend of the biomedical use of SMAs. Auricchio *et al.* [2021] presented an overview of the use of SMAs for cardiovascular surgery, which minimizes the size of devices, impact procedures and recovery time, making this an interesting approach to investigate. Pfensig *et al.* [2018] presented numerical simulations of a transcatheter aortic heart valve using SMAs. Ashuri *et al.* [2020] discussed perspectives related to the use of biomedical

soft robots. Jiang *et al.* [2020] evaluated SMA-based sheath for minimally invasive surgery. Li *et al.* [2019] developed a bioinspired soft actuator composed by SMA and silicon rubber for crawling and grasping. Liu *et al.* [2020] used shape memory polymers to build metamaterial-based stent, a biomedical device employed to avoid vascular blockage. Lee and Kang [2021] presented a review of the shape memory polymers and the design strategies for biodegradable shape memory polymers. Applications related to self-expanding stents, drug-eluting systems and tissue engineering are treated and studies that aim to reduce the time response of SMAs stents and their combination with drug release ability are of concern. Safaei *et al.* [2021] discussed the biomedical applications of NiTi alloys by employing additive manufacturing process.

Porous SMA has been employed for biomedical applications due to its biocompatibility, motivating applications in medical implants, surgical instruments, among others. Zhu *et al.* [2020] developed a constitutive model for porous shape memory alloys. Song *et al.* [2021] promoted an evaluation of the mechanical properties and clinical application of SMA scaphoid arc nail. Werner *et al.* [2020] discussed experimental validation of SMA screw implants. Wu *et al.* [2019] presented an overview about the use of SMA staples for fracture fixation.

Prostheses are one of the important bioinspired systems where tensegrity idea can be exploited. Human foot prosthesis has the objective to accommodate the weight during walking while maintaining the kinematics functions of the foot. On this basis, McNicholas *et al.* [2018] investigated the mechanical behavior of several prostheses designed for high activity performance. The authors reported that prosthetic foot with more compliant behavior appeared to provide more late-stance energy return compared to high stiffness ones, which means that the more energy is reutilized in the next step. The study also suggests that more compliant foot prostheses reduce metabolic cost of high demanding activities. On the other hand, Klodd *et al.* [2010] experimentally showed that high stiffness foot prosthesis tends to significantly reduce ankle dorsiflexion, and as intuitively expected, provides less late-stance energy recovery. Hence, this indicates a trade-off between natural movement and energy recovery of the prosthetic foot.

This paper deals with the use of smart tensegrity structures to develop a human foot prosthesis. The idea is to combine proper mechanical properties with adaptive behavior, where SMA actuation mimics the continuous tendon/muscle action. A quasi-static nonlinear mechanics investigation is carried out considering a minimal regular tensegrity prism with SMA strings. The tensegrity structure is modeled by the force density matrix approach based on node mapping. Numerical simulations are developed from an optimization procedure employing the Levenberg–Marquardt method. The SMA thermomechanical behavior is described by considering a polynomial constitutive model that allows the description of the two-way shape memory effect. The constitutive equation is based on the original polynomial model proposed by Falk [1980]. An investigation of the tensegrity capability to model a human foot

is carried out. The biotensegrity prosthesis performance is compared with high performance prostheses available on the market, showing that it is an interesting alternative. In addition, human foot physiology is investigated by considering the SMA actuation to promote different foot movements showing the prosthesis capability to mimic a human foot. The use of the tensegrity structures to develop foot prosthesis is novel, and the use of SMA actuation opens a new promising field of investigation. Besides that, the complex model involved to deal with these aspects constitutes another contribution.

2. Mathematical Model

This section presents the mathematical model for the description of tensegrity prisms. Mechanical quasi-static analysis is provided by considering a general formulation applied to any tensegrity prism, with any number of polygon sides. A general

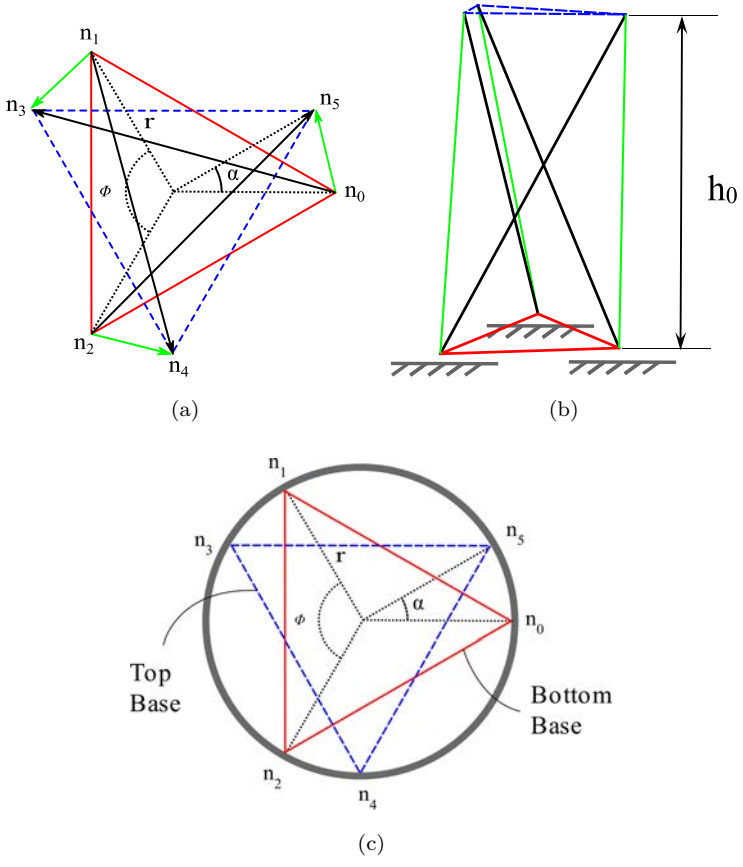

Fig. 1. Minimal regular tensegrity prism with $p = 3$, $r_t = r_b = r$: (a) top view; (b) frontal view; (c) triangle base circumscribed by a virtual circle of radius r. (adapted from [Skelton and Oliveira, 2009]).

stable three-dimensional tensegrity prism can be built using p bars, with p-sided polygons of horizontal strings on the top and on the bottom, and vertical strings on the sides. The minimal regular tensegrity prism is the one that uses the smallest number of strings ($3p$) to promote stabilization, namely p horizontal-top strings, p horizontal-bottom strings, and p vertical strings. An example of the geometrical characteristic of the simplex tensegrity is presented in Fig. 1 considering $p = 3$ (triangles) and nodes $n_0 \ldots n_5$. The bars are represented by black lines; the vertical strings are represented by green lines; the top horizontal strings are represented by blue dotted lines; and the bottom horizontal strings are red lines. The top and bottom polygons are parallel and equilateral, being circumscribed by virtual circles that can present different radius from each other, r_t and r_b. Therefore, the geometric characteristics of the tensegrity structure are the virtual circle radius, assumed to be equal, r; the initial height, h_0; the characteristic angle, ϕ; and the torsion angle, α. For more details about the tensegrity modeling, see Skelton and Oliveira [2009] and Zhang and Ohsaki [2015].

The mathematical notation considers bold lowercase symbols for vectors, bold uppercase symbols for matrices, and italic symbols for scalars.

In addition to tensegrity modeling, SMA, thermomechanical behavior, is described by considering a polynomial constitutive model [Falk, 1980, 1983].

2.1. *Tensegrity equilibrium*

The equilibrium of a general tensegrity structure can be established by mapping forces and displacements by considering representative matrices. Basically, each column of the matrix is related to a node while each line is associated with a direction. In this regard, considers that matrix $\mathbf{W}$ represents the internal forces and $\mathbf{F}$ represents the external forces [Skelton and Oliveira, 2009],

$$\mathbf{W} - \mathbf{F} = \mathbf{0} \tag{1}$$

Force density matrix approach decomposes the internal forces, $\mathbf{W}$, as functions of the displacements, $\mathbf{X}$:

$$\mathbf{W} = \mathbf{W}(\mathbf{X}) \tag{2}$$

The displacement matrix $\mathbf{X}$ is calculated by mapping node positions, establishing a relation between the current and the initial node positions. Therefore, the displacements are written as functions of the node configuration

$$\mathbf{X} = \mathbf{X}(\mathbf{N}) \tag{3}$$

where $\mathbf{N}$ are the node coordinates. Based on that, we have

$$\mathbf{W} = \mathbf{W}(\mathbf{N}) \tag{4}$$

Under these assumptions, internal forces can be written as follows:

$$\mathbf{W} = \mathbf{N}\mathbf{C}^{\mathbf{T}}\mathbf{Q}\mathbf{C} \tag{5}$$

where $\mathbf{C}$ is the connectivity matrix that can be understood as a transformation matrix that represents node interconnection; the diagonal force density matrix $\mathbf{Q}$ contains the force per unit of length for each one of the m structure members, depending on the constitutive relations. Therefore, equilibrium is established as follows:

$$\mathbf{NC^T QC - F = 0} \tag{6}$$

Holonomic constraints are of concern which means that they are explicitly time independent. In order to define the constraints, consider a vector $\widetilde{\mathbf{h}}$ where each component is picked up from the nodal matrix $\mathbf{N}$ defining restricted nodes in specific directions. Therefore, each component of the vector $\widetilde{\mathbf{h}}$ is associated with a constraint condition defined by a vector $\widetilde{\mathbf{h}}^c$. On this basis, vector $\mathbf{g}$ is built containing the constraint conditions, being expressed as follows:

$$g_k = \widetilde{h}_k - \widetilde{h}_k^c = 0 \quad (k = 1, \ldots, n_c) \tag{7}$$

where the subscript k represents the kth constraint condition for a specific direction of a node. $\widetilde{h}_k$ is the node coordinate being restricted, and $\widetilde{h}_k^c$ is the node coordinate that is assumed to be the same of $\widetilde{h}_k$, which means that node vanishes its displacement on the constrained direction. A mapping matrix $\mathbf{M}$ is employed to identify the constrained node and its direction associated with the nodal matrix $\mathbf{N}$.

Lagrange multipliers, λ_k, are employed to represent constraints [Frankel, 2012; Hand and Finch, 1998] by adding functions of the form $\lambda_k g_k(\mathbf{N})$ to the system Lagrangian. Since the constraint function is defined as a nodal displacement constraint, the constraint force vector of a specific node direction is given by

$$\frac{\partial(\lambda_k g_k)}{\partial g_k} = \lambda_k \tag{8}$$

The total constraint force matrix $\mathbf{S}$ acting on the tensegrity structure is the composition of all reaction forces for each constrained node, being assembled by placing the Lagrange multipliers on its corresponding position indicated by the mapping matrix $\mathbf{M}$. Incorporating the reaction forces through the addition of the constraint matrix on the equilibrium equations gives:

$$\mathbf{W - F + S = 0} \tag{9}$$

On this basis, the governing equations incorporating equilibrium and constraints are described by $6p + n_c$ equations instead of the $6p$ equilibrium equations:

$$\begin{cases} \mathbf{w - f + s = 0} \\ \mathbf{g = 0} \end{cases} \tag{10}$$

where $\mathbf{f} = \text{vec}(\mathbf{F})$, $\mathbf{w} = \text{vec}(\mathbf{W})$ and $\mathbf{s} = \text{vec}(\mathbf{S})$ with vec( ) representing vectorization operator, which transforms a matrix into a column vector by stacking the columns of the operated matrix on top of each other.

By considering an extended vector $\boldsymbol{\omega}$ consisting of $\mathbf{w} - \mathbf{f} + \mathbf{s}$ and $\mathbf{g}$, it is written a compact representation:

$$\boldsymbol{\omega} = \begin{Bmatrix} \mathbf{w} - \mathbf{f} + \mathbf{s} \\ \mathbf{g} \end{Bmatrix} = \mathbf{0} \tag{11}$$

The Levenberg–Marquardt method is a good alternative to deal with this problem [Chong and Żak, 2008; Yuan *et al.*, 2017], solving an optimization problem defined by an objective function associated with a norm of the vector $\boldsymbol{\omega}$: $f_{\text{obj}} = \|\boldsymbol{\omega}\|^2$.

2.2. *SMA thermomechanical model*

The most important phenomena related to the SMA thermomechanical behavior are the pseudoleasticity and shape memory effect (or one-way shape memory effect). Pseudoleastic effect occurs at high temperature where austenitic phase is stable in a stress-free state. Under this condition, a stress field induces phase transformation from austenite to a martensitic variant. The removal of the stress field induces the reverse transformation, defining a stress–strain hysteresis loop. Shape memory effect occurs at low temperature where martesitic phase is stable in the absence of stress field. A mechanical load promotes a martensitic reorientation and the load removal is associated with a residual strain that can be eliminated by a subsequent temperature increase. Therefore, a proper thermomechanical load induces an original shape recover that can be exploited for different purposes.

The two-way shape memory effect (TWSME) is a phenomenon that confers the SMA the ability to associate a specific shape to each temperature, making possible to remember their original shape even without the application of mechanical loads. The TWSME is achieved by a training process performed through thermomechanical cycles that induces macroscopic observable permanent changes in the material behavior. The TWSME training process creates a residual internal stress state that facilitates the formation of preferred martensitic variants induced by temperature changes in the absence of mechanical loads [Lagoudas, 2008].

The thermomechanical description of SMAs can be dealt by different constitutive models. Paiva and Savi [2005], Lagoudas [2008] and Cisse *et al.* [2016] presented overviews of the constitutive models for SMAs. In this work, the polynomial model due to Falk [1980, 1983] is chosen since it provides a simple alternative that represents the general thermomechanical behavior of SMAs, being able to capture the main phenomena for the biotensigrity description. This polynomial model is based on the Landau–Ginzburg–Devonshire theory and the idea is to define a polynomial free energy potential function capable to describe pseudoelasticity and shape memory effect. In this regard, the polynomial equation is based on stabilities of the SMA macroscopic phases: austenite (A) and two variants of martensite (tension, M+, and compression, M–). On this basis, it is considered that SMA has two stable phases for low temperature, bellow T_M, representing two martensitic variants; three stable phases for intermediate temperature ($T_M < T < T_A$), representing two martensitic

variants and austenite; and just one stable phase for high temperature (above T_A) representing austenite. Hence, the polynomial model is defined considering a free energy that is represented by a sixth- order polynomial as a function of strain and temperature as follows:

$$\psi = \frac{a(T - T_M)\varepsilon^2}{2} - \frac{b\varepsilon^4}{4} + \frac{b^2}{4a(T_A - T_M)}\frac{\varepsilon^6}{6} \tag{12}$$

where ε is the strain and T is the SMA temperature; a and b are material parameters; T_A is the temperature at which austenite is stable above, T_M is the temperature at which martensite is stable below.

The stress–strain–temperature relation is defined by the following equation:

$$\sigma^{SMA} = a(T - T_M)\varepsilon - b\varepsilon^3 + \frac{b^2}{4a(T_A - T_M)}\varepsilon^5 \tag{13}$$

This model represents the thermomechanical equilibrium curve and can be understood as nominal events occurring as a consequence of the equilibrium instabilities that yields bifurcations of the response in the stress–strain curve. A calibration with experimental data due to Tobushi *et al.* [1991] is of concern using parameters of Table 1.

Figure 2 presents energy curves for three different temperature levels showing the maximum–minimum characteristics related to each one of the macroscopic phases. Figure 3 shows the polynomial model together with experimental data where it is

Table 1. Polynomial model parameters adjusted from experimental results due to Tobushi *et al.* [1991].

T_A (K)	T_M (K)	a (MPa/K)	b (MPa)	σ_p (MPa)
361.25	295	530	159×10^5	50

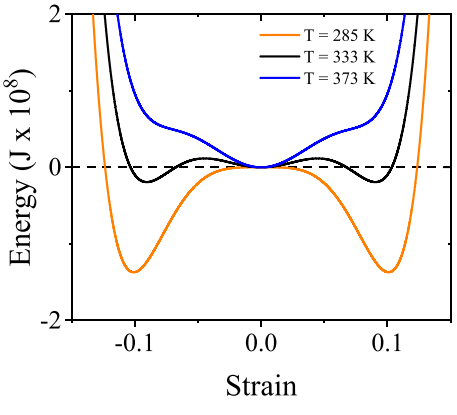

Fig. 2. Helmholtz free energy for different temperatures showing the maximum and minimum points associated with the SMA macroscopic phases.

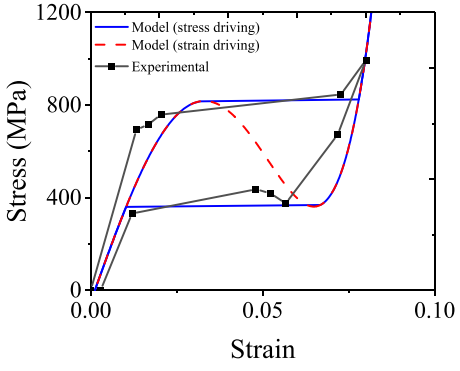

Fig. 3. Polynomial model representing pseudoelastic behavior compared with experimental data due to Tobushi *et al.* [1991].

noticeable that strain driving case represents the equilibrium configuration while stress driving case represents hysteresis.

The two-way shape memory effect can be described by including a residual stress σ_p that represents the internal stress state promoted by the training process [Rodrigues *et al.*, 2017a, Rodrigues *et al.*, 2017b]. Based on that, the force–displacement–temperature relation is given by the following equation:

$$F^{\mathrm{SMA}} = \frac{A}{L}\left[a(T - T_M)u - bu^3 + \frac{b^2}{4a(T_A - T_M)}u^5 - \sigma_p\right] \tag{14}$$

where σ_p is a residual stress induced by the two-way shape memory effect training process; A is the cross-section area and L is the length.

Figure 4 presents the shape memory effect showing the one-way and two-way cases. Figure 4(a) presents the force–displacement–temperature curve of the one-way shape memory effect for the force driving case. Basically, a mechanical loading

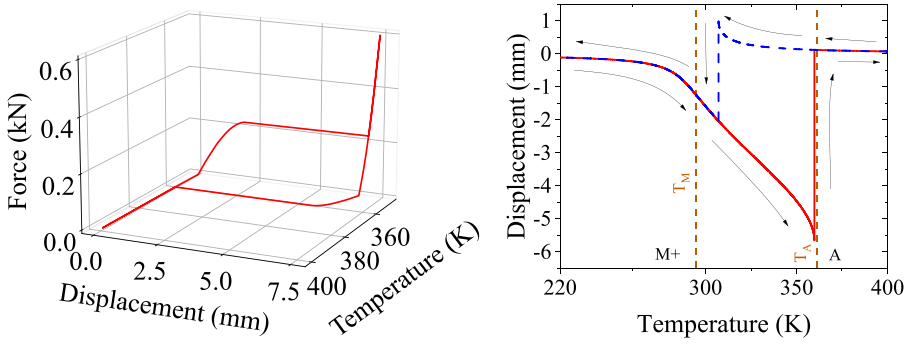

(a) (b)

Fig. 4. SMA polynomial model for shape memory effect: (a) one-way shape memory effect; (b) two-way shape memory effect with $\sigma_p = 50\,\mathrm{MPa}$.

is applied to the SMA element and after the unloading process, SMA presents a residual strain that can be recovered by a thermal cycle. Figure 4(b) presents the displacement–temperature curve of the two-way shape memory effect for a temperature driving case showing that shape change is promoted by a thermal cycling – in the absence of a mechanical load. It is noticeable that phase transformations are occurring from the martensitic variant M+ to the austenitic phase, A.

A convenient way of heating the strings is using electric current through Joule effect. Therefore, the following equation is employed to describe the relationship between the temperature and electric current:

$$T = \frac{i_w^2 R_w}{m_w c_w} + T_0 \tag{15}$$

where T_0 is the initial temperature of the SMA, i_w is the electric current, R_w is the resistance, m_w is the mass and c_w is the specific heat of the SMA actuator.

3. Biotensegrity Foot Model

This section exploits the use of a biotensegrity structure to represent a human foot with its main features and characteristics. The human foot is a complex body member composed by bones, ligaments, tendons and muscles. Figure 5 presents foot representations through a schematic picture of a human left foot and a sagittal cross section.

According to Khale *et al.* [1986], the weight distribution on the foot is characterized by the foot print — presented in Fig. 6 as a shaded area — that can be interpreted as the supporting surface provided by the soft tissues. This surface has three main contact points, called bony support points, represented by the calcaneal tuberosity (point 0), the head of the fifth metatarsal (point 1) and the head of the first metatarsal bones (point 2), forming a triangle called plantar arch (red triangle).

Muscles, ligaments and tendons have an essential function on the foot physiology, being characterized by elastic nature. Figure 7 presents some details of the foot concerning the ligaments. According to Khale *et al.* [1986], foot ligaments are divided into groups: the ones that join the leg bones to each other and to the tarsals (cyan); the ones that join the talus to the other tarsals (blue); the remaining dorsal ligaments (magenta); the plantar tarsal ligaments (red) that connect the individual tarsals on their plantar surfaces; the ligaments between the tarsus and the metatarsus (purple); and the ligaments between the metatarsals (green). These ligaments constitute the foot medial, sagittal (transversal) and lateral arches, resulting in triangle shape form between the arches. More details can be found in traditional anatomy, physiology and atlases of the human body, as for instance: Sobotta *et al.* [2011], Faller *et al.* [2004] and Khale *et al.* [1986].

A biotensegrity structure is proposed in order to represent the main foot features. Three main structural aspects are of concern establishing an analogy between the

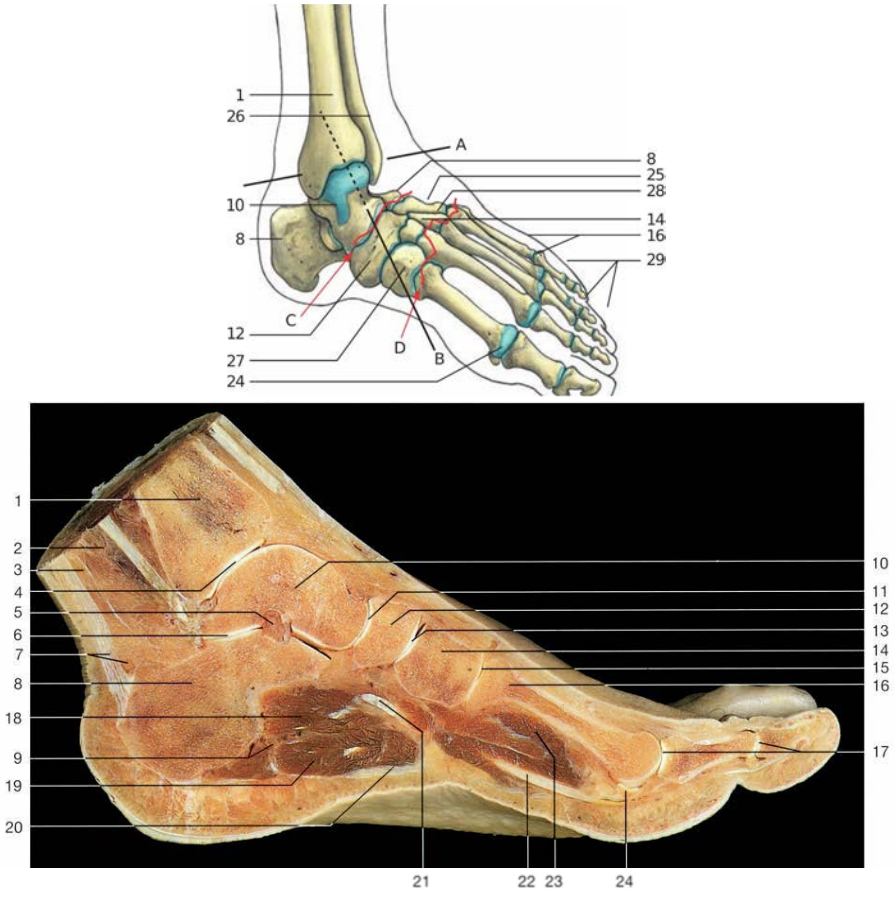

Fig. 5. Human foot represented by a schematic picture of the skeleton of the left foot where joints are indicated in blue and red lines are the axis of joints; sagittal section through the foot [Rohen *et al.*, 2015].

human foot and the biotensegrity structure: the weight distribution performed by the bones and its relationship with the tensegrity rigid elements; the ligaments of the foot and their relationship with the tensegrity elastic elements; and the physiology of the foot and its relationship with the tensegrity capability to mimic foot movements.

A simplex tensegrity structure is employed using the plantar arch as its bottom base. Muscles, ligaments and tendons are represented by the tensegrity strings. The biotensegrity is schematically presented in Fig. 8 showing that the plantar arch is used to accommodate the bars of the tensegrity structure as the bony foot bearing weight points. Figure 9 shows the ligament arches of interest leading to the accommodation of the strings of the tensegrity structure to represent the ligaments of the foot. Finally, this leads to the construction of a biotensegrity structure with a triangle base.

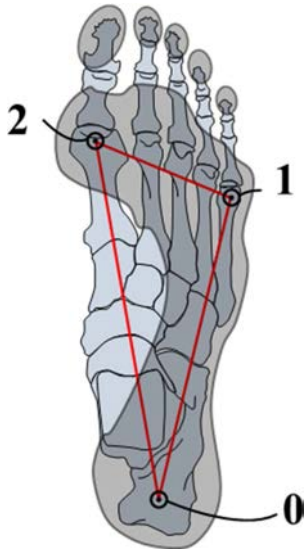

Fig. 6. Foot weight bearing points represented by three main contact points, called bony support points: the calcaneal tuberosity (point 0), the head of the fifth metatarsal (point 2) and the head of the first metatarsal bones (point 2).

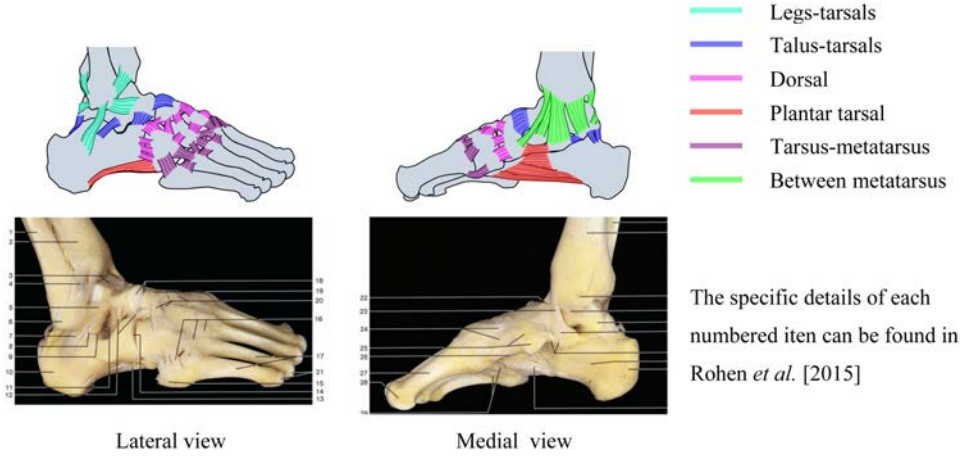

Fig. 7. Ligaments of the human foot.

The geometrical characteristic of the simplex biotensegrity is presented in Fig. 1 and in Table 2 that also presents the bar stiffness, k_b, which is necessary to represent the biotensegrity mechanics [Skelton and Oliveira, 2009; Zhang and Ohsaki, 2015]. Biotensegrity parameters are adjusted with experimental data due to Amendola *et al.* [2014], together with SMA parameters due to Rodrigues *et al.* [2017a, 2017b].

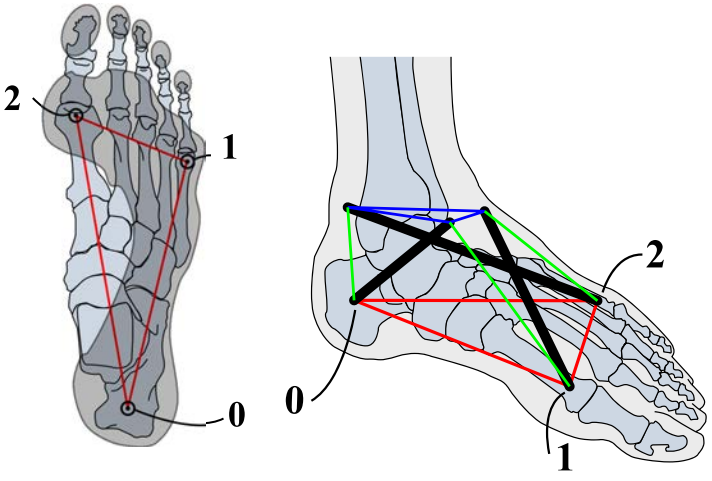

Fig. 8. Foot bony arches and simplex biotensegrity model.

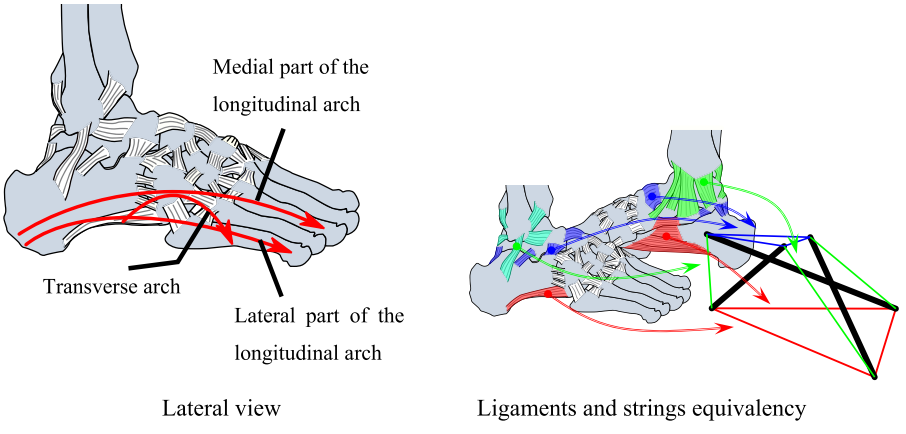

Fig. 9. Foot ligament arches and their equivalency to the biotensegrity strings.

Table 2. Simplex tensegrity parameters adjusted from experimental parameters due to Amendola *et al.* [2014] and SMA parameters adjusted from Tobushi *et al.* [1991] experimental results and SMA pre-stress from Rodrigues *et al.* [2017a, 2017b].

r (m)	h_0 (m)	α	ϕ	A (mm^2)	k_b (kN/m)
0.081	0.077	30°	60°	0.5	42810.3
T_A(K)	T_M(K)	a (MPa/K)		b (MPa)	σ_p (MPa)
361.25	295	530		159×10^5	50

4. Prosthesis Mechanical Analysis

The biotensegrity mechanical performance is now of concern, establishing a comparison with the available market prostheses, observing force and stiffness. Experimental work of McNicholas *et al.* [2010] is used as reference where the compliant forefoot keel structure is of concern considering the following commercial prosthetic feet: Thrive (Freedom Innovations, Irvine, CA); Trekk (Makstride Prosthetics, Prescott, AZ); Panthera CFII (mediUSA, Whitsett, NC); Triton Heavy Duty (Otto Bock, Duderstadt, Germany); Rush Foot (Ability Dynamics, Tempe, AZ); Renegade AT (Freedom Innovations, Irvine, CA); Variflex XC (Össur, Reykjavik, Iceland); All Pro (Fillauer, Chattanooga, TN); and Soleus Tactical (College Park, Warren, MI).

Figure 10 shows the experimental set up employed by McNicholas *et al.* [2010] considering prosthetic feet in a used state, tested with a 20° angle to follow the ISO 10328 standard. The test loaded the foot up to body weight of three individuals plus a 22 kg of a supposed carried weight. This extra weight simulates the weight carried by the users while in duty.

Biotensegrity foot prosthesis performance is now of concern by considering a loading process similar to the cited experimental test represented by an external load with a 20° inclined with respect to the z-axis load. A rotation matrix is employed to rotate the load vector around the y-axis. Figure 11 presents force–displacement curves and the physical structure configurations, showing the initial and final configurations using a reference temperature $T = 400\,\mathrm{K}$ and a prestress of 80 N for the SMA strings. Note that the force distribution is heterogeneous, and each bar has different responses. Bar 3 has a hardening behavior while bar 2 has a hardening followed by a softening behavior; bar 1 has the same behavior of bar 3, but with a more intense softening. Since the main load acting on a foot is vertical, even though there are horizontal components, an interesting parameter to be analyzed is the

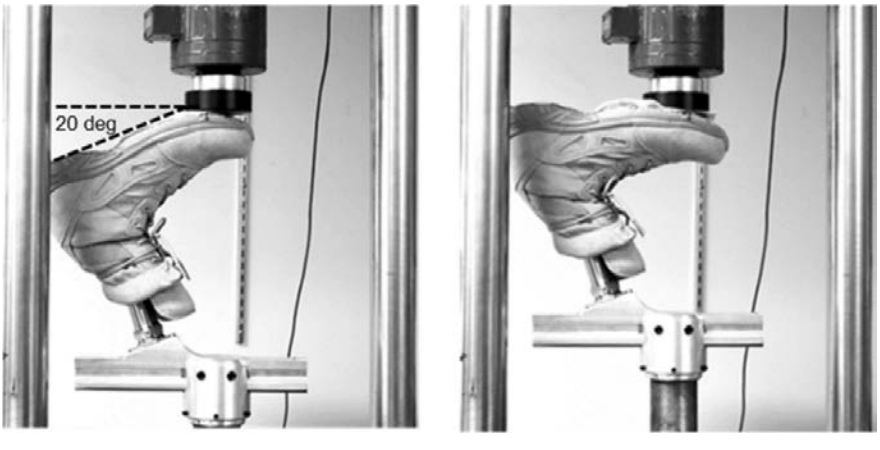

Fig. 10. Experimental set used by McNicholas *et al.* [2010].

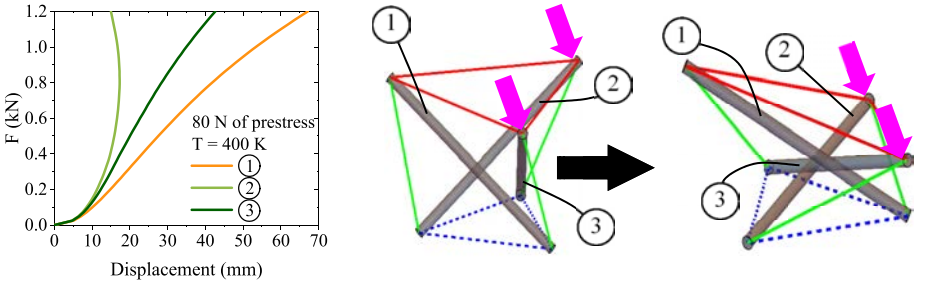

Fig. 11. Tensegrity structure subjected to an inclined load analysis; bars are indicated by circled numbers.

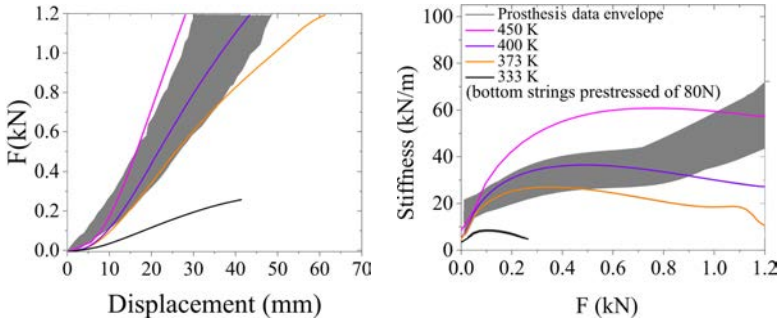

(a) (b)

Fig. 12. Commercial prostheses and biotensegrity performance comparison considering different prestressed tensegrity structures [McNicholas *et al.*, 2010]: (a) force–displacement curves; (b) stiffness curves.

height of the structure. For this purpose, one can track the height of the geometric center of the base prism to represent the height displacement of the whole structure.

A comparison between the commercial prostheses and the biotensegrity is now in focus. For the sake of succinctness, an envelope containing results of the experimental tests due to McNicholas *et al.* [2010] is considered as reference to represent all the analyses. Figure 12 presents a comparison among commercial prostheses and biotensegrity prosthesis, where different temperatures on the top and bottom strings are analyzed, while the vertical strings are at 333 K. Figure 12(a) shows the force–displacement curves while Fig. 12(b) shows the stiffness of each one of them. It is noticeable that the biotensegrity structure presents a similar performance considering both the force and the stiffness.

5. Prosthesis Physiology Analysis

Biomimicry of the foot physiology is performed by considering SMA actuation induced by temperature variations of the strings to represent the action of muscles,

Table 3. Actuation imposed to perform the foot movement.

Movement	Bottom nodes restricted to the ground	Constant temperature on the unactuated strings	Position of the actuated vertical string	Initial (T_0) and final temperature on the vertical actuated strings
Dorsiflexion	Node 0	333 K	Nodes 1 and 2	333–350 K
Varus	Nodes 0 and 2	333 K	Node 1	333–350 K
Eversion	Nodes 0 and 1	333 K	Node 2	333–350 K
Plantarflexion	Nodes 1 and 2	333 K	Node 0	333–350 K

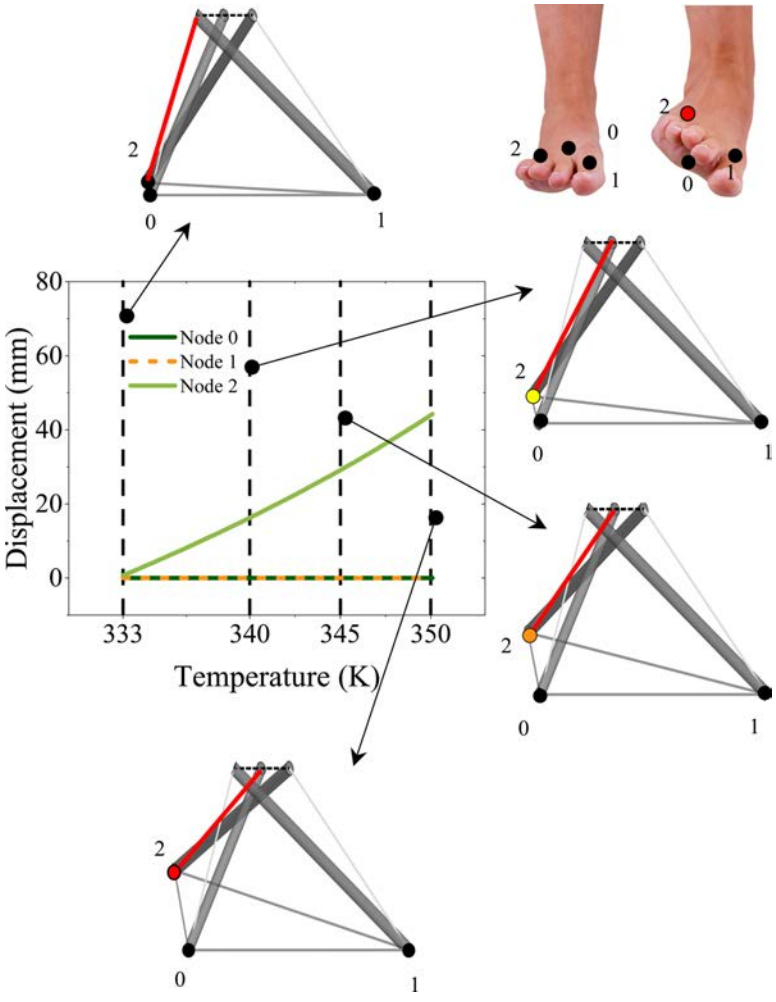

Fig. 13. Tensegrity structure temperature–displacement response for replicating eversion foot movement.

ligaments and tendons. Typical foot movements are represented: mid-stance, plantar-flexion, dorsiflexion, eversion and varus. Initially, equilibrium configuration is reached by assuming an 80 N prestress of the horizontal top strings, with an initial temperature $T_0 = 333\,\mathrm{K}$, and the bottom nodes are restricted to the ground on the z-axis. Afterward, movements are induced considering changes on the node restrictions in such a way that the top nodes are completely restricted (x, y and z-axis) and specific bottom nodes are connected to the ground, without movement. Actuation is carried out exploiting the SMA two-way shape memory effect induced by temperature variations of the vertical strings that are increased to 350 K.

Table 3 summarizes SMA actuation for each one of the movements that are treated in the sequel.

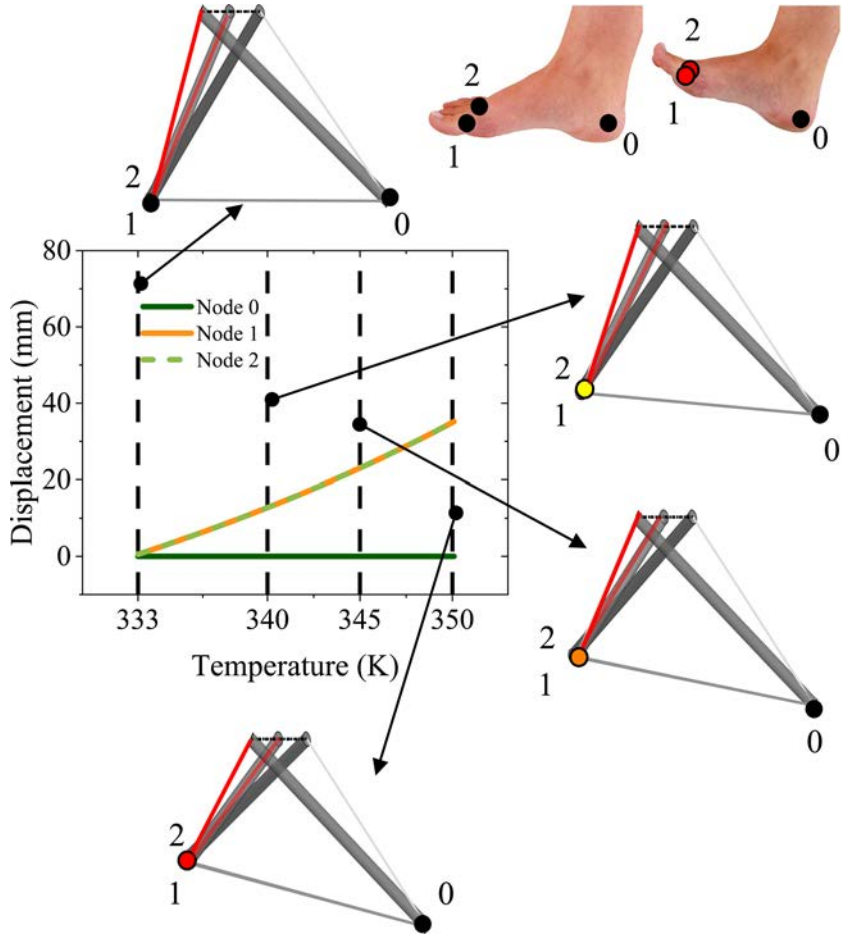

Fig. 14. Tensegrity structure temperature–displacement response for replicating dorsiflexion foot movement.

Figure 13 shows the biotensegrity structure performing the eversion foot movement, induced by the heating of the vertical string attached to node 2 from 333 to 350 K (identified by red color), where node 2 starts rising until it reaches the final configuration. A schematic picture of the foot movement is presented and four structure configurations are shown from four different temperatures: 333, 340, 345 and 350 K. Note that either the structure configuration or the temperature–displacement curves show that nodes 0 and 1 do not rise, since their vertical attached string is not actuated. The schematic picture of foot shows the corresponding foot movement, where the left part of the fore foot (original position of node 2) is lifted from the floor.

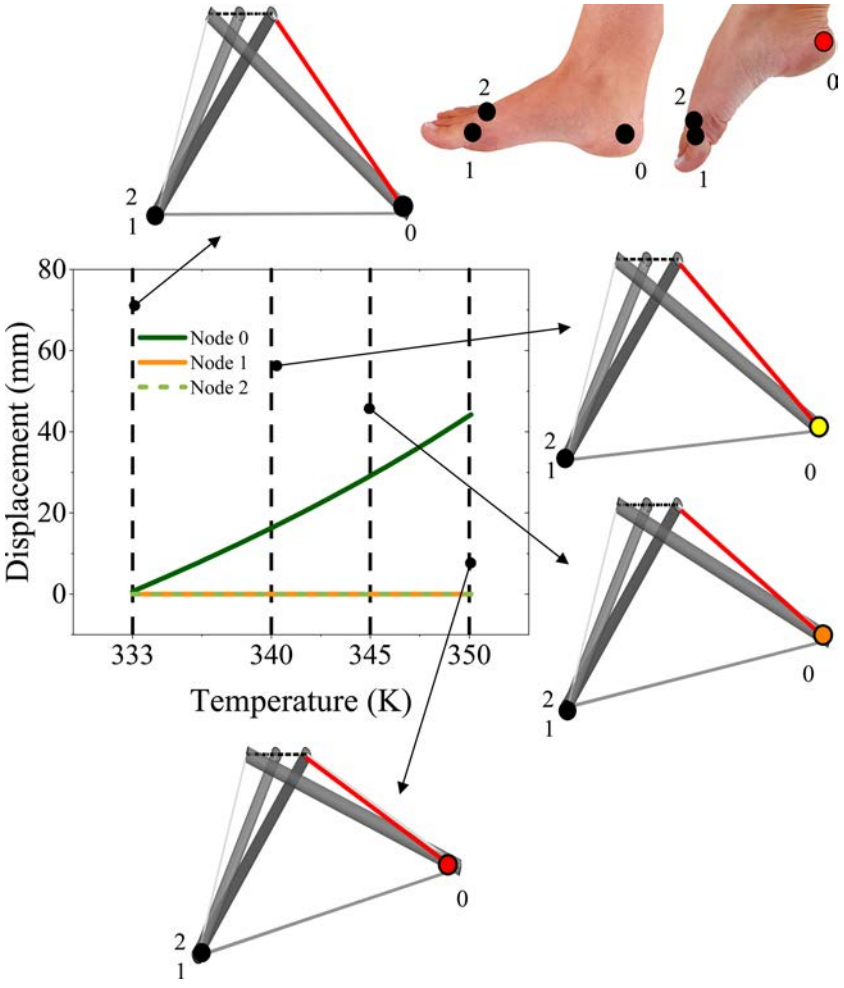

Fig. 15. Tensegrity structure temperature–displacement response for replicating plantarflexion foot movement.

Figure 14 shows the biotensegrity structure performing the dorsiflexion movement by heating the vertical string attached to nodes 1 and 2 from 333 to 350 K. Nodes 1 and 2 start rising until they reach the final configuration and node 0 does not rise since its vertical attached string is not actuated. Moreover, the fore foot — related to nodes 1 and 2 — is lifted from the floor.

Figure 15 shows the biotensegrity structure performing the plantarflexion movement by heating the vertical string attached to node 0 from 333 to 350 K. Node 0 starts rising until it reaches the final configuration, and the left part of the hind foot — where node 0 is located — is lifted from the floor.

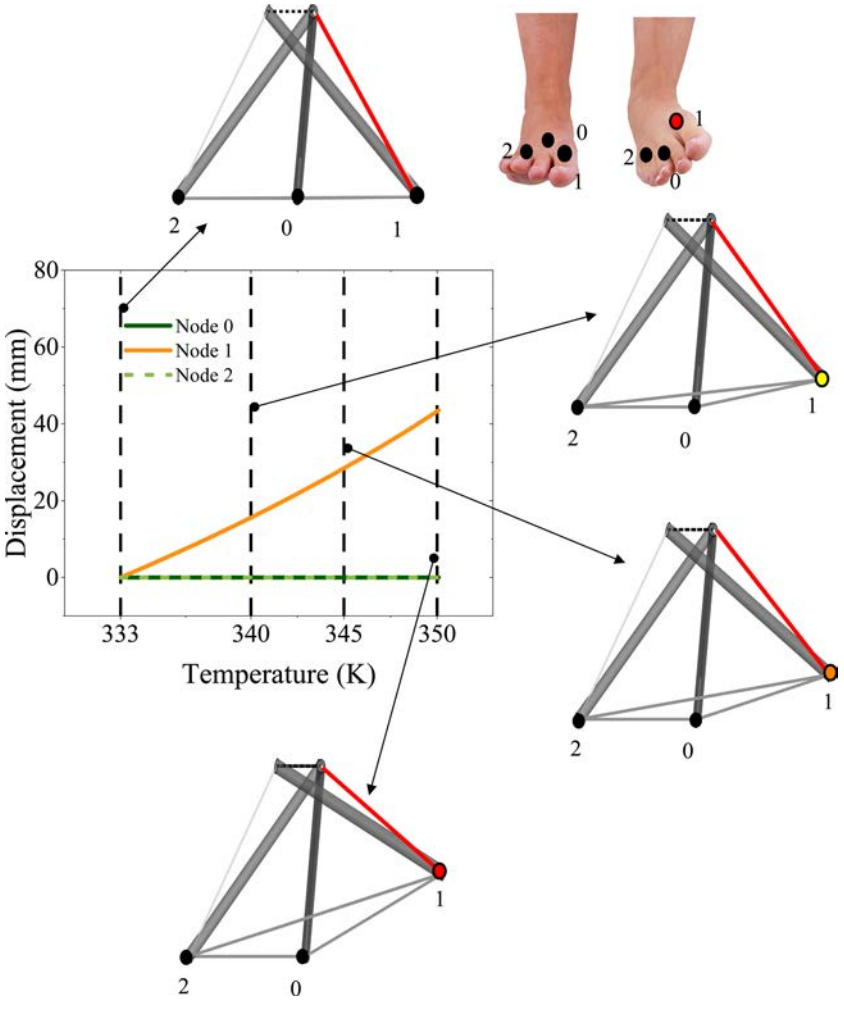

Fig. 16. Tensegrity structure temperature–displacement response for replicating varus foot movement.

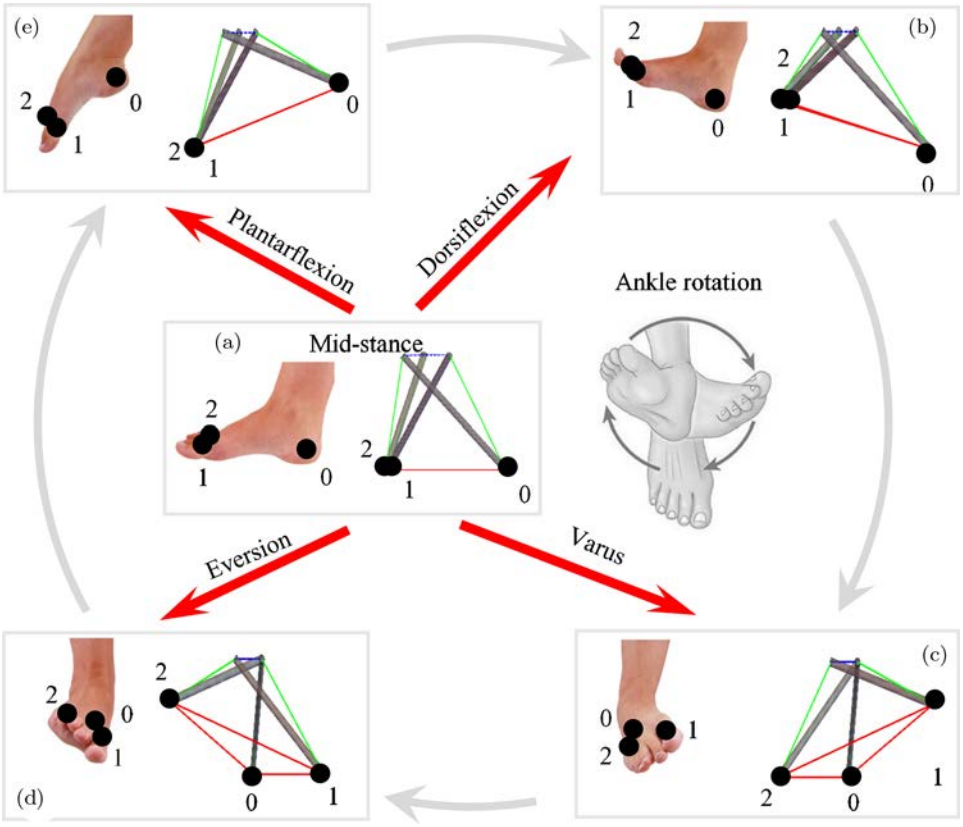

Fig. 17. Biotensegrity foot movements mimicry induced by SMA actuation: (a) mid-stance; (b) dorsiflexion; (c) varus; (d) eversion; (e) plantarflexion. (foot images from [Ianuzzi and Mkandawire, 2016]).

Figure 16 shows the biotensegrity structure performing the varus movement, by heating the vertical string attached to node 1 from 333 to 350 K. Node 1 starts rising until it reaches the final configuration showing that the right part of the fore foot — where node 1 is located — is lifted from the floor. Note that nodes 0 and 2 do not rise.

Figure 17 summarizes the foot physiology actuated by SMAs starting from the mid-stance position and showing mid-stance, plantar-flexion, dorsiflexion, eversion and varus.

6. Conclusions

This work deals with the nonlinear mechanics of a biotensegrity human foot prosthesis actuated by shape memory alloys (SMAs). Tensegrity structure is modeled

by considering the force density matrix approach and numerical simulations are performed by the Levenberg–Marquardt optimization procedure. SMA actuation is modeled by considering a polynomial constitutive model, modified to incorporate the description of the two-way shape memory effect. The biotensegrity foot model is based on the triangle base similar to the weight distribution of the foot, being capable of representing its physiology. A comparison between the foot biotensegrity with high performance prostheses available on the market is carried out. The biotensegrity presents similar mechanical performance considering both the force and the stiffness. Foot physiology is mimicked by considering SMA actuation that is able to produce different foot movements: mid-stance, plantar-flexion, dorsiflexion, eversion and varus. The prosthesis capacity to mimic foot movements and its mechanical performance show that the simplex biotensegrity has an interesting potential to be used as foot prosthesis. This work presents a proof of concept that should be confirmed by additional experimental investigations.

Acknowledgments

The authors would like to acknowledge the support of the Brazilian Research Agencies CNPq, FAPERJ and CAPES.

References

Amendola, A., Carpentieri, G., de Oliveira, M., Skelton, R. E and Fraternali, F. [2014] "Experimental investigation of the softening–stiffening response of tensegrity prisms under compressive loading," *Composite Structures* **117**, 234–243, doi:10.1016/j.compstruct.2014.06.022.

Ashuri, T., Armani, A., Jalilzadeh Hamidi, R., Reasnor, T., Ahmadi, S. and Iqbal, K. [2020] "Biomedical soft robots: Current status and perspective," *Biomedical Engineering Letters* **10**, 369-385, doi:10.1007/s13534-020-00157-6.

Auricchio, F., Conti, M., Stefania, M., Morganti, S. and Scocozza, F. [2021] "SMA cardiovascular applications and computer-based design," in *Shape Memory Alloy Engineering For Aerospace, Structural, and Biomedical Applications*, eds. N. Concilio and V. Antonucci, 2nd edn (Elsiver, Amsterdam), doi:10.1016/B978-0-12-819264-1.00020-0.

Benyus, J. M. [1997] *Biomimicry* (Cambridge University Press, Cambridge).

Buckminster Fuller, R. [1962] Tentional Integrity Structures US3139957A Patent.

Cañadas, P., Laurent, V. M., Oddou, C., Isabey, D. and Wendling, S. [2002] "A cellular tensegrity model to analyse the structural viscoelasticity of the cytoskeleton," *Journal of Theoretical Biology* **218**, 155–173. doi:10.1006/jtbi.2002.3064.

Chong, E. K. P. and Żak, S. H. [2008] *An Introduction to Optimization* (John Wiley and Sons, Hoboken, NJ, USA), doi:10.1002/9781118033340.

Cisse, C., Zaki, W. and Ben Zineb, T. [2016] "A review of constitutive models and modeling techniques for shape memory alloys," *International Journal of Plasticity* **76**, 244–284, doi:10.1016/j.ijplas.2015.08.006.

Deepak Bansod, Y., Nandanwar, D. and Burša, J. [2014] "Overview of tensegrity — I: Basic structures," *Engineering Mechanics* **21**, 355–367.

Ekeberg, Ö. and Pearson, K. [2005] "Computer simulation of stepping in the hind legs of the cat: An examination of mechanisms regulating the stance-to-swing transition," *Journal of Neurophysiology* **94**, 4256–4268, doi:10.1152/jn.00065.2005.

Falk, F. [1980] "Model free energy, mechanics, and thermodynamics of shape memory alloys," *Acta Metallurgica* **28**, 1773–1780, doi:10.1016/0001-6160(80)90030-9.

Falk, F. [1983] "Ginzburg-Landau theory of static domain walls in shape-memory alloys," *Zeitschrift für Physik B Condensed Matter* **51**, 177–185, doi:10.1007/BF01308772.

Faller, A., Schünke, M. and Schünke, G. [2004] *The Human Body* (Georg Thieme Verlag, Stuttgart, Germany), doi:10.1055/b-005-148851.

Frankel, T. [2012] "Holonomic and nonholonomic constraints," *Journal of Geometry and Physics* 165–188, doi:10.1017/cbo9781139061377.011.

Hand, L. N. and Finch, J. D. [2013] *Analytical Mechanics* (Cambridge University Press, Cambridge, England).

Hutson, M. and Ward, A. [2003] *Musculoskeletal Medicine*, 2nd edn. (Oxford University Press, Oxford), doi:10.5694/j.1326-5377.1990.tb126282.x.

Ianuzzi, A. and Mkandawire, C. [2016] "Applications of UHMWPE in total ankle replacements," in *UHMWPE Biomaterials Handbook: Ultra High Molecular Weight Polyethylene in Total Joint Replacement and Medical Devices*, 3rd edn. (Elsevier, Amsterdam), doi:10.1016/B978-0-323-35401-1.00013-2.

Jian, S., Chen, B., Qi, F. Cao, Y., Ju, F., Bai, D. and Wang, Y. [2021] "A variable-stiffness continuum manipulators by an SMA-based sheath in minimally invasive surgery," *International Journal of Medical Robotics and Computer Assisted Surgery* **16**, e2081.

Klodd, E., Hansen, A., Fatone, S. and Edwards, M. [2010] "Effects of prosthetic foot forefoot flexibility on gait of unilateral transtibial prosthesis users," *Journal of Rehabilitation Research and Development* **47**, 899–910, doi:10.1682/JRRD.2009.10.0166.

Koehler-McNicholas, S. R., Nickel, E. A., Barrons, K., Blaharski, K. E., Dellamano, C. A., Ray, S. F., Schnall, B. L., Hendershot, B. D. and Hansen, A. H. [2018] "Mechanical and dynamic characterization of prosthetic feet for high activity users during weighted and unweighted walking," *PLoS One* **13**, 1–16, doi:10.1371/journal.pone.0202884.

Lagoudas, D. C. [2008] *Shape Memory Alloys*: *Modeling and Engineering Applications* (Springer, New York).

Lee, J. and Kang, S. K. [2021] "Principles for controlling the shape recovery and degradation behavior of biodegradable shape-memory polymers in biomedical applications," *Micromachines* **12**, doi:10.3390/mi12070757.

Li, Z., Huang, R. and Liu, Z. [2019] "A periodic deformation mechanism of a soft actuator for crawling and grasping," *Advanced Materials Technologies* **4**, 1–10, doi:10.1002/admt.201900653.

Liu, R., Xu, S., Luo, X. and Liu, Z. [2020] "Theoretical and numerical analysis of mechanical behaviors of a metamaterial-based shape memory polymer stent," *Polymers* (*Basel*) **12**, doi:10.3390/polym12081784.

Motro, R. [2003] *Tensegrity*, *Structural Systems for the Future* (Kogan Page Limited, London).

Oliveira, M. C. and Skelton, R. E. [2009] "Tensegrity systems," *Journal of Chemical Information and Modeling*, doi:10.1007/978-0-387-74242-7.

Paiva, A. and Savi, M. A. [2006] "An overview of constitutive models for shape memory alloys," *Mathematical Problems in Engineering*, 1–30, doi:10.1155/MPE/2006/56876.

Passino, K. M. [2006] "Biomimicry for optimization, control, and automation," *IEEE Control Systems*, doi:10.1109/MCS.2006.1657880.

Paulsen, Friedrich and Waschke, J. [2018] *Sobotta Atlas of Human Anatomy*, 15th edn (Fischer Gustav Verlag, New York, NY).

Pfensig, S. Kaule, S., Ott, R., Wustenhagen, C., Stiehm, M., Keiler, J., Wree, A., Grabow, N., Schmitz, K.-P. and Siewert, S. [2018] "Numerical simulation of a transcatheter aortic heart valve under application-related loading," *Current Directions in Biomedical Engineering* **4**(1), 185–189.

Rodrigues, G. V., Fonseca, L. M., Savi, M. A. and Paiva, A. [2017] "Nonlinear dynamics of an adaptive origami-stent system," *International Journal of Mechanical Sciences* **133**, 303–318, doi:10.1016/j.ijmecsci.2017.08.050.

Rodrigues, G. V., Fonseca, L. M. and Savi, M. A. [2017] "Dynamics of a self-folding cylindrical system actuated by SMA," doi:10.26678/abcm.cobem2017.cob17-2655.

Rohen, J. W., Yokochi, C. and Edition, E. [2015] *Anatomy a Photographic Atlas, Color Atlas of Anatomy a Photographic Study of the Human Body* (Igaku-Shoin Medical Publishers Ltd, Tokyo).

Safaei, K., Abedi, H., Nematollahi, M., Kordizadeh, F., Dabbaghi, H., Bayati, P., Javanbakht, R., Jahadakbar, A., Elahinia, M. and Poorganji, B. [2021] "Additive manufacturing of NiTi shape memory alloy for biomedical applications: Review of the LPBF process ecosystem," *JOM* **73**, 3771–3786, doi:10.1007/s11837-021-04937-y.

Savi, M. A., Paiva, A., de Araujo, C. J. and de Paula, A. S. [2016] "Shape memory alloys," in *Dynamics of Smart Systems and Structures* (Springer International Publishing, Cham), pp. 155–188, doi:10.1007/978-3-319-29982-2_8.

Scarr, G. [2012] "A consideration of the elbow as a tensegrity structure," *International Journal of Osteopathic Medicine* **15**, 53–65, doi:10.1016/j.ijosm.2011.11.003.

Simmons, A. H., Michal, C. A. and Jelinski, L. W. [2010] "Molecular orientation and two-component nature of the crystalline fraction of spider dragline silk published by: American association for the advancement of science stable," *Advanced Science* **271**, 84–87, http://www.jstor.org/stable/2890379.

Song, M., Su, Y., Li, C. and Xu, Y. [2021] "Evaluation of the mechanical properties and clinical application of nickel–titanium shape memory alloy scaphoid arc nail," *Engineering in Life Sciences* **21**, 294–302.

Sultan, C., Stamenović, D. and Ingber, D. E. [2004] "A computational tensegrity model predicts dynamic rheological behaviors in living cells," *Annals of Biomedical Engineering* **32**, 520–530, doi:10.1023/B:ABME.0000019171.26711.37.

Sun, J., Song, G., Chu, J. and Ren, L. [2019] "An adaptive bioinspired foot mechanism based on tensegrity structures," *Soft Robot* **6**, 778–789, doi:10.1089/soro.2018.0168.

Termonia, Y. [1994] "Molecular modeling of spider silk elasticity," *Macromolecules* **27**, 7378–7381, doi:10.1021/ma00103a018.

Tobushi, H., Iwanaga, N., Tanaka, K., Hori, T. and Sawada, T. [1991] "Deformation behavior of Ni–Ti shape memory alloy subjected to variable stress and temperature," *Continuum Mechanics and Thermodynamics* **3**, 79–93.

Vera, C., Skelton, R., Bossens, F. and Sung, L. A. [2005] "3-D nanomechanics of an erythrocyte junctional complex in equibiaxial and anisotropic deformations," *Annals of Biomedical Engineering* **33**, 1387–1404, doi:10.1007/s10439-005-4698-y.

Werner, M., Hammer, N., Rotsch, C., Berthold, I. and Leimert, M. [2020] "Experimental validation of adaptive pedicle screws — a novel implant concept using shape memory alloys," *Medical and Biological Engineering and Computing*, **58**, 55–65.

Wu, J. C., Mills, A., Grant, K. D. and Wiater P. J. [2019] "Fracture fixation using shape-memory (Nitinol) staples," *Orthopedic Clinics of North America* **50**(3), 367–374.

Yuan, X. F., Ma, S. and Jiang, S. H. [2017] "Form-finding of tensegrity structures based on the Levenberg–Marquardt method," *Computers & Structures* **192**, 171–180, doi:10.1016/j.compstruc.2017.07.005.

Zhang, J. Y. and Ohsaki, M. [2015] *Tensegrity Structures, Tensegrity Structures* (Springer, New York).

Zhu, X., Chu, L. and Dui, G. [2020] "Constitutive modeling of porous shape memory alloys using Gurson–Tvergaard–Needleman model under isothermal conditions," *International Journal of Applied Mechanics* **12**, 1–21, doi:10.1142/S1758825120500386.